PCCP

Cite this: *Phys. Chem. Chem. Phys.*, 2012, **14**, 5489–5503

www.rsc.org/pccp

PAPER

Vibrations and hydrogen bonding in porphycene†

Sylwester Gawinkowski,[a] Łukasz Walewski,*[b] Alexander Vdovin,[c] Alkwin Slenczka,[c] Stephane Rols,[d] Mark R. Johnson,[d] Bogdan Lesyng[ef] and Jacek Waluk*[a]

Received 22nd December 2011, Accepted 20th February 2012
DOI: 10.1039/c2cp24098j

Combined use of IR, Raman, neutron scattering and fluorescence measurements for porphycene isolated in helium nanodroplets, supersonic jet and cryogenic matrices, as well as for solid and liquid solutions, resulted in the assignments of almost all of 108 fundamental vibrations. The puzzling feature of porphycene is the apparent lack of the N–H stretching band in the IR spectrum, predicted to be the strongest of all bands by standard harmonic calculations. Theoretical modeling of the IR spectra, based on *ab initio* molecular dynamics simulations, reveals that the N–H stretching mode should appear as an extremely broad band in the 2250–3000 cm^{-1} region. Coupling of the N–H stretching vibration to other modes is discussed in the context of multidimensional character of intramolecular double hydrogen transfer in porphycene. The analysis can be generalized to other strongly hydrogen-bonded systems.

1. Introduction

Specific spectral and photophysical characteristics, as well as an essential role played by porphyrins in many biological processes, make these compounds attractive for promising applications in various fields.[1] Porphycene (Pc), a constitutional isomer of porphyrin (Scheme 1), differs from the latter in several aspects. The electronic absorption of Pc and its derivatives in the low energy range is about an order of magnitude stronger than in the parent compound; a similar enhancement is observed for fluorescence quantum yield.[2,3] On the other hand, triplet state formation is less efficient, but sufficient enough to generate singlet oxygen with yields exceeding 30%, which makes porphycenes good candidates for photodynamic therapy.[4]

With regard to fundamental research, tautomerism in porphyrins and porphycenes has attracted much attention.[5–36]

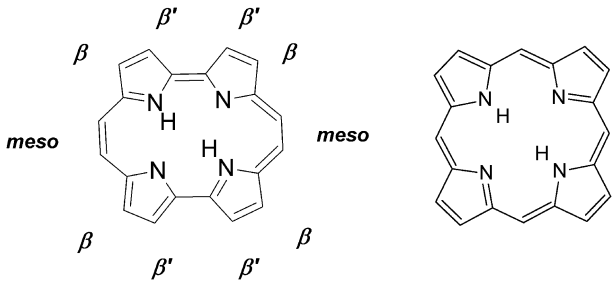

Scheme 1 Porphycene (left) and porphyrin (right).

Both shape and size of the internal cavity formed by four nitrogen atoms are different in the two molecules, which results in the two intramolecular N–H···N hydrogen bonds being much stronger for Pc. This has immense consequences for the tautomerization rates. The two internal hydrogens in Pc move back and forth between two chemically equivalent *trans* structures (Scheme 2) with the rate of 5.8×10^{11} s^{-1} at room temperature.[22] The corresponding rate for porphyrin is many orders of magnitude lower (2600 s^{-1} at 267 K).[8] Also the mechanisms of tautomerization are different. In porphyrin, the reaction proceeds in a stepwise manner, starting from thermally activated tunneling of single hydrogen. This leads to the *cis* tautomer, which, upon second single hydrogen transfer can form the final *trans* tautomer, or revert to the initial *trans* form.[5–7] The experimental and theoretical evidence for porphycene suggests a concerted, albeit not necessarily synchronous mechanism.[16–18,22,29,30] Actually, for *meso*-substituted porphycenes, where both *trans* and *cis*-1 forms were detected, the experiment showed that the *trans–trans* conversion is faster than the *cis–trans* process.[19]

[a] *Institute of Physical Chemistry, Polish Academy of Sciences, Kasprzaka 44, 01-224 Warsaw, Poland. E-mail: waluk@ichf.edu.pl; Fax: +48 22 3433333; Tel: +48 22 3433332*
[b] *Interdisciplinary Centre for Mathematical and Computational Modelling, University of Warsaw, Pawińskiego 5a, 02-106 Warsaw, Poland. E-mail: ljw@icm.edu.pl*
[c] *Institut für Physikalische und Theoretische Chemie, Universität Regensburg, Universitätsstraße 31, 93053 Regensburg, Germany. E-mail: Alkwin.Slenczka@chemie.uni-regensburg.de*
[d] *Institut Laue-Langevin, Grenoble, France. E-mail: johnson@ill.fr*
[e] *Department of Biophysics, Faculty of Physics, University of Warsaw, Zwirki i Wigury 93, 02-089 Warsaw, Poland. E-mail: B.Lesyng@icm.edu.pl*
[f] *Bioinformatics Laboratory, Mossakowski Medical Research Centre, Pawinskiego 5, 02-106 Warsaw, Poland*
† Electronic supplementary information (ESI) available: Details of normal mode calculations, computed vibrational frequencies, forms of vibrational modes. See DOI: 10.1039/c2cp24098j

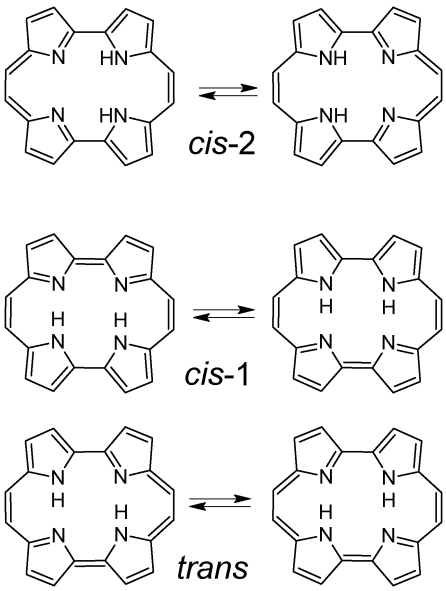

Scheme 2 Tautomeric forms of Pc.

The studies of Pc in the regime of molecular isolation, either in supersonic jets[15,31] or in helium nanodroplets,[20] revealed tunneling splittings in electronic absorption and fluorescence, due to delocalization of the internal hydrogens. These splittings are vibrationally mode-selective. For some vibrations the value of splitting, 4.4 cm^{-1}, is practically the same as that determined for the 0–0 transition. However, for a low frequency 180 cm^{-1} mode, the splitting exceeds 12 cm^{-1}, the increase reflecting the form of the vibration, which brings the hydrogen-bonded N atoms closer to each other, thus lowering the tautomerization barrier (see ESI† or Fig. 8 for atomic displacements from the equilibrium structure in this mode, 2 AG). For yet another low frequency mode, which effectively decreases the hydrogen bonding strength (1 AG, ESI† or Fig. 8), the splitting becomes undetectably low (<0.1 cm^{-1}). These findings point to the important role of tunneling and indicate a multidimensional character of tautomerization in porphycene, confirmed by theoretical studies.[18,24,27,34–36] In a work devoted to identifying vibrational modes relevant for the proper description of the potential governing the motion of the inner protons, Kühn and co-workers used four-dimensional and six-dimensional nuclear wavefunctions, the latter for a singly deuterated isotopologue.[35]

Naturally, the key to understanding the complex mechanism of tautomerization in Pc is the knowledge of the intramolecular hydrogen bond (HB) parameters. Usually, a measure of the HB strength is provided by the frequency of the N–H stretching vibration. Surprisingly, previous IR studies of porphycene[10] revealed no trace of the N–H stretching band, even though it was predicted by both DFT and RHF calculations to be the most intense in the whole IR spectrum. Moreover, the authors stated that the IR, Raman and fluorescence data are not conclusive enough to determine whether the *trans* form is really dominant, as suggested by the calculations.

The experiments based on polarization spectroscopy performed for Pc in the last decade[12,14,22,25,29,30,32,33] leave little doubt that the lowest energy form corresponds to the *trans* tautomer, at least for parent Pc. However, except for a series of papers devoted to the resonance Raman spectra of porphycene anions,[37–40] no progress has been reported regarding vibrational structure. The goal of the present work was, therefore, to assign in detail the vibrations in porphycene, with particular attention to the modes involved in the intramolecular hydrogen bonds. For this purpose, we have performed IR, Raman, fluorescence and inelastic neutron scattering (INS) experiments for the parent Pc and for its doubly-deuterated isotopologue, Pc-d_2, in which the inner protons were replaced by deuterons. Regarding theoretical studies, going beyond the harmonic model seemed mandatory. We therefore carried out extensive *ab initio* molecular dynamics simulations, aimed at understanding coupling between vibrational modes in porphycene.

The results allow us to propose a solution for the porphycene puzzle, to understand the apparent lack of a strong N–H band in the IR spectrum, and to discuss the coupling between low and high frequency modes in porphycene.

2. Experimental and theoretical methods

Porphycene was synthesized and purified according to literature procedures.[41,42] The doubly deuterated isotopologue was obtained by dissolving the compound in the $CH_3OD/CHCl_3$ mixture and subsequent evaporation of the solvent. Perdeuteration of Pc was achieved by heating the compound in 70% D_2SO_4 in D_2O for 24 h. After that, chloroform was added to the cooled solution before being neutralized with diluted $NaOD/D_2O$. Finally, the organic layer was concentrated *in vacuo*. The degree of deuteration was checked by mass spectra and was estimated to be higher than 90%.

The solvents (CCl_4 and CS_2, IR grade, acetone, spectroscopic grade, all from Aldrich) were used without further purification. KBr powder (IR grade, Aldrich) was dried for 4 h at 250 °C before use.

The infrared spectra were measured on a Nicolet Magna 560 FT spectrometer, equipped with a MCT/B liquid-nitrogen-cooled detector or on a Nicolet 170SX, using InSb 2 and MCT liquid-nitrogen-cooled detectors. For the far-IR region, the measurements were made using a Nicolet 20F FT spectrometer with a DTGS (room temperature) detector using polyethylene pellets.

At room temperature, the spectra were recorded for solutions, KBr or polyethylene pellets, or thin solid films on KBr windows. The spectra at low-temperature were obtained for Pc embedded in solid argon, nitrogen or xenon, obtained by deposition of matrices on a cold KBr window of a closed-cycle helium cryostat (CSW-202 N, Advanced Research Systems). A typical guest–host ratio was about 1 : 10^3. The deposition could be monitored by on-line collection of IR spectra.

The Raman spectra were taken with an InVia Renishaw Raman spectrometer based on a Leica microscope equipped with 100×, 50×, 20×, 5× objectives for visible and a 15× objective for UV excitation, 1200, 1800 and 2400 grooves mm^{-1} gratings, and a thermoelectrically cooled CCD array detector. Three laser lines were used: 785 nm (HPNIR785), 514.5 nm (Stellar Pro argon Modu-Laser, LLC), and 325 nm (He–Cd Kimmon laser). The laser power on the sample was kept below 0.1 mW. The spectral resolution was 5 cm^{-1} and the wavenumber accuracy was ±2 cm^{-1}, both calibrated with the Rayleigh line

and the 520.6 cm^{-1} line of silicon. The samples were checked for thermal decomposition; whenever necessary, it was avoided by defocussing or lowering the laser power.

Dispersed emission spectra of Pc-d_0 and Pc-d_2 were taken in a helium droplet machine. The droplet source was built according to the design developed in Göttingen.[43,44] Helium droplets were generated in a supersonic expansion of helium gas (grade 6.0) through a 5 mm orifice. The stagnation pressure was 20 bar and the source temperature was 11 K, which leads to an average droplet size of 20 000 helium atoms.[45] Pc was doped into the helium droplets by the pick-up technique. Thereby, the droplet beam was passed through an oven, where a solid sample of Pc was heated for sublimation. The temperature was tuned to optimize for single molecule doping of the droplets. Further downstream, the doped droplet beam was irradiated by a single mode ring dye laser (Coherent 899-29 Autoscan II) tuned to the electronic origin of the dopant species (16 145.92 cm^{-1} for Pc-d_0, and 16 101.67 cm^{-1} for Pc-d_2). The fluorescence was collected by a quartz lens and imaged onto the entrance slit of a grating spectrograph (SPEX). The detector was a charge coupled device (CCD) camera (Andor, DU 401-BV) with a 256 × 1024 CCD chip operated in the vertical binning mode. Thus, a spectrum consisting of 1024 data points was accumulated with a spectral resolution of 0.7 cm^{-1} per pixel. The frequency scale was calibrated with an Ar–Ne lamp using the literature data.[46]

INS spectra were measured on two spectrometers. The direct geometry, thermal neutron, time-of-flight (TOF) spectrometer, IN4,[47] was used to measure the low frequency spectrum, including the elastic peak. A Cu220 monochromator was used to give an incident wavelength of 0.9 Å (E = 100 meV) allowing Stokes' spectrum to be measured up to almost 100 meV in the temperature range from 10 K to 300 K. In this configuration the energy resolution (FWHM) is about 3% of the energy transfer. The neutron TOF is used to measure the energy of scattered neutrons. The pyrolitic graphite monochromator (PG002) was used to give an incident wavelength of 2.7 Å (E = 11 meV) and a better energy resolution (FWHM) of ~1 meV which is approximately constant across the spectrum. With lower energy neutrons, anti-Stokes' spectrum was measured in the temperature range from 150 K to 300 K for which the excited vibrational levels are sufficiently well-populated up to about 50 meV.

Spectra from 30 meV up to 500 meV were measured using the inverse geometry, beryllium filter spectrometer, IN1.[48] The final energy is fixed by the beryllium filter at 3 meV. A spectrum is obtained by varying the incident wavelength, which is achieved by scanning the take-off angle of the crystal monochromator, in this case Cu220. Energy resolution (FWHM) is approximately 2% of energy transfer. Spectra were measured at 10 K and 200 K.

Samples were mounted in aluminium sachets of height and width (4 cm and 3 cm, respectively) chosen to intercept the whole neutron beam. Sample thickness was not more than 1 mm. Reflection geometry for the sample was chosen, its orientation being 135° to the incident beam. Standard orange cryostats were used for temperature control, the precision being better than ±1 K at all temperatures. The four isotopologues, Pc-d_0, Pc-d_2, Pc-d_{12} and Pc-d_{14}, were measured on both spectrometers. The data treatment was performed using the LAMP program,[49] in particular for the integration of IN4 data to produce generalized densities of states.

Quantum-chemical calculations were carried out using Gaussian 03 and Gaussian 09 program packages. The equilibrium geometry of Pc in the electronic ground state was optimized at the B3LYP/6-31G(d,p) and B3LYP/6-311++G(fd,2dp) levels. This was followed by harmonic frequency calculations and normal mode analysis (NMA). Simulated fluorescence spectra were obtained using the Franck–Condon approximation as implemented in Gaussian 09 package. We will refer to the results obtained with those methods as "harmonic", opposed to "anharmonic", as discussed later in the text.

Born–Oppenheimer molecular dynamics simulations were carried out at the DFT level of theory as implemented in the CPMD package.[50] Gradient-corrected exchange-correlation functional (BLYP) was used.[51,52] The valence electron wavefunction was expanded in the plane wave (PW) basis up to 70 Ry, and the interactions of core electrons were described using the norm conserving pseudopotentials.[53] The Poisson equation was solved using the Hockney method[54] in a simple cubic simulation cell with the side length of 15 Å. Decoupling of the periodic images for the electrostatic interactions was applied using cluster boundary conditions.[69] The 3rd order predictor–corrector extrapolation of the wave function was applied to decrease the number of SCF cycles required to converge wavefunction gradients down below 5×10^{-6} a.u. Nuclear equations of motion were integrated using the symplectic velocity Verlet algorithm with the time-step of 20 a.u. (~0.48 fs). Center of mass motion was subtracted every 0.5 ps.

The IR spectra were computed according to the following protocol. The system was initially equilibrated at 300 K using one Nosé–Hoover chain thermostat of length 3 per degree of freedom.[55] 100 ps long NVT trajectory was generated using the same massive thermostating scheme. The positions and velocities were selected from this trajectory at 2 ps intervals and used as initial conditions for 45 independent NVE simulations, each 20 ps long. The total dipole moment was computed at each MD step along all the NVE runs. In the post-processing phase the Fourier transform of the classical autocorrelation function of the total dipole moment was computed for each trajectory. The quantum correction factor was applied to obtain the IR lineshape function.[56] The resulting IR spectra were averaged over all 45 NVE simulations providing the canonical ensemble average at 300 K. The same protocol was applied to three Pc isotopologues, Pc-d_0, Pc-d_1 and Pc-d_2. Normal mode analysis (NMA) was carried out using the same settings as those used for MD simulations, yielding normal mode frequencies f_i (see Table S1, ESI†) and normal mode vectors $\boldsymbol{e}_i$. The vectors $\boldsymbol{e}_i$ were assigned to those obtained at the B3LYP/6-31G(d,p) level to obtain a consistent mapping between the theoretical and the experimental vibrations (see ESI† for the details of this assignment).

Mass-weighted projections $p_i(t)$ of the molecular trajectories $\boldsymbol{r}(t)$ onto the normal mode vectors $\boldsymbol{e}_i$ were computed according to the formula $p_i(t) = \boldsymbol{M}\boldsymbol{r}(t)\cdot\boldsymbol{e}_i$ ($\boldsymbol{M}$ being the diagonal matrix of square roots of atomic masses $\sqrt{m_i}$) to obtain 108 projected normal mode (PNM) signals. Power spectra $p_i(\omega)$ of the PNMs were computed using Fourier transform, and the dominant

peaks were fitted with Lorentz functions. Median μ_i of the ith fit was taken as the effective frequency $\nu_i = \mu_i/2\pi$ corresponding to the mode i (see Table S1, ESI†). The frequencies ν_i match the IR peak positions and can be used to assign molecular motions $\boldsymbol{e}_i$ to the IR spectral features. We name these frequencies *anharmonic* because they were obtained without invoking harmonic approximation to the electronic potential.

3. Results and discussion

Porphycene has 108 vibrations (see ESI† for the forms of all normal modes). The C_{2h} symmetry of the planar *trans* tautomeric forms dictates that eighteen AU and thirty six BU modes should be IR-active, whereas in the Raman and fluorescence spectra, transitions involving thirty seven AG and seventeen BG modes are allowed. Inspection of IR and Raman spectra shows that the mutual exclusion principle is strictly obeyed, which provides a strong argument for the *trans* structure of Pc. This finding also allows a separate analysis of modes of *gerade* and *ungerade* symmetry.

3.1 IR-active vibrations

Comparison of the experimental results and the theoretical predictions is presented in Table 1 and Fig. 1 and 2. The IR spectra have been previously reported for Pc embedded in KBr and CsI pellets and cryogenic nitrogen matrices.[10] We have measured the IR spectra for polycrystalline Pc, KBr pellets, low-temperature nitrogen and xenon matrices, and, additionally, the IR absorption for Pc solutions. The latter helps in cases where the observed multiplet structure may be due to matrix sites or crystal splittings. Most importantly, we recorded the spectra of both undeuterated Pc (Pc-d_0) and the isotopologue in which the inner protons have been replaced by deuterons (Pc-d_2). Finally, we also carried out initial studies on Pc-d_{12}, a molecule with all protons except the two internal ones replaced by deuterons. Besides providing information on vibrations involving N–H/N–D bonds, comparison of experimental and theoretical results for isotopologues improves the reliability of the assignments, because the isotopic shifts are usually computed with better accuracy than the absolute energies of vibrational transitions. Additional support was provided by the INS spectra, which turned out to be particularly useful in the low energy region. The agreement between observed and calculated transitions is impressive (see Fig. 1 and 2), regarding not only the band locations, but also relative intensities. In the case of harmonic frequencies practically the same scaling factors were obtained for the parent and doubly deuterated Pc, using all the fundamental transitions lying below 1600 cm^{-1}. No significant changes in the predicted spectral patterns were observed when the basis set was increased from 6-31G(d,p) to 6-311++G(fd,2dp); slightly larger scaling factors were obtained for the larger basis set, 0.975 for Pc-d_0 and 0.973 for Pc-d_2, compared with 0.968 and 0.966 obtained while using 6-31G(d,p). The RMS errors were about 8 cm^{-1} for Pc-d_0 and 10 cm^{-1} for Pc-d_2. In principle, these errors could have been made even smaller by applying different scaling factors for modes of different type, an approach used before for porphyrin.[57–59] We did not attempt such a procedure, since it would not lead to changes in the vibrational assignments.

We propose the assignments for 52 out of 54 computed vibrational transitions of *ungerade* symmetry. One of the missing vibrations, 1 AU, is of very low frequency and therefore lies outside the spectral range of our instruments. On the contrary, the other one, 30 BU, corresponds to the asymmetric N–H stretch and was computed as the most intense IR band. This striking discrepancy between experiment and harmonic calculations prompted us to extend the theoretical studies to the model that goes beyond harmonic approximation. As will be shown below, the apparent lack of the N–H stretch in the experimental spectrum can be explained by an extreme breadth of this transition, due to the coupling to other vibrational modes.

We could, on the other hand, identify another vibration involved in the intramolecular hydrogen bond, the asymmetric N–H out-of-plane bending (18 AU). It was observed at 964–971 cm^{-1} (depending on the environment) in Pc-d_0 and red-shifted by 282 cm^{-1} in Pc-d_2, in very good agreement with the computational predictions. The calculations also correctly reproduce the decrease in intensity observed for the deuterated derivative. Interestingly, the band position and intensity of this vibration change markedly in different environments. Such behavior, characteristic of the out-of-plane N–H mode, has been described previously.[60–62]

The transition energy for the out-of-plane N–H bending mode is exceptionally high, indicating strong N–H···N hydrogen bonds. For dibenzo[*b*,*i*][1,4,8,11]tetraaza[14]annulene (TAA), another molecule with the same structural motif of the inner cavity composed of four nitrogens (see Scheme 3), we have observed the corresponding band at 778 cm^{-1}, shifting to 599 cm^{-1} in the deuterated species.[63] For porphyrin, B3LYP/6-31G(d,p) calculations predict two vibrations with contributions from the asymmetric N–H out-of-plane wagging, located at 748 and 808 cm^{-1}. The experiment shows two modes at 785 and 731 cm^{-1} which are affected by deuteration.[57,64,65] In the doubly deuterated porphyrin molecule, a band appears at 540 cm^{-1} which can be assigned to the N–H wagging vibration. In a classic work on the IR spectra of porphyrins,[66] Mason identified the "out-of-plane deformation" bands in the parent and -d_2 porphyrins at 719 and 537 cm^{-1}, respectively. It is interesting to note very similar values of the shifts in TAA and in porphyrin, but a significantly larger value for porphycene, which provides another argument for high intramolecular HB strength in this molecule.

It is well known for porphyrin that no single transition can be assigned to the C–N–H in-plane bending vibration. Several in-plane modes are affected by deuteration, as evidenced by spectral shifts.[64] A similar behavior is observed for Pc. The IR absorption patterns for Pc-d_0 and Pc-d_2 are quite similar in the region below 1100 cm^{-1}, but strongly differ in the 1100–1600 cm^{-1} range. The calculations predict significant contributions of N–H bending for as many as six modes in the range of 1200–1600 cm^{-1} (Table 1). In Pc-d_2, the N–D bending mainly contributes to two modes, 11 BU and 12 BU, with transition energies around 1000 cm^{-1}. This different distribution of the NH/ND bending contributions is the main reason why the forms of some vibrations in the two isotopologues do not follow a 1 : 1 correlation pattern. According to theoretical studies, most of the modes do not significantly change their form after double deuteration. Those that do, correspond to the in-plane

Table 1 Observed and computed modes of *ungerade* symmetry

Pc-d_0										Pc-d_2				
Observed[a]							Calculated[b]			Observed	Calculated			Assignment[d]
KBr	CCl_4	CS_2	Solid PC[c]	N_2	Xe	INS[c]	Symm	$\tilde{\nu}$	Int	KBr	Symm	$\tilde{\nu}$	Int	
							1 AU	61	0		1 AU	61	0	o tilt
						93	2 AU	72	1.9		2 AU	72	2	o tilt
						108	3 AU	89	5.2		3 AU	88	4.8	o tilt
225						224	4 AU	206	1.1		4 AU	206	1.2	o tilt
232							1 BU	237	2.6		1 BU	236	2.5	i im ph b
303							5 AU	311	0.7		5 AU	311	0.7	o ph C10H C20Hb
314						315	6 AU	320	1.7		6 AU	320	1.7	o im C9H C19H b
320							2 BU	323	3.4		2 BU	322	3.3	i bp bend
384						387	3 BU	391	15.5		3 BU	390	15.9	as ip im-ph s
464		464	463				4 BU	472	16.6	459	4 BU	468	15.7	i im ph b
						509	7 AU	512	0		7 AU	512	0	o *meso*-CH b
624		618	624	625	622		5 BU	626	2.3	623	5 BU	625	2.5	i skel def
					630		8 AU	640	0.8		8 AU	639	0	o Cβ′H b
653			653				6 BU	673	17.3	642	6 BU	663	17.2	i skel def
658	657	656	655	655	655	663	9 AU	674	11.3	680	9 AU	664	24.2	o CH b
698		694	698	698	696		10 AU	714	0.7		10 AU	709	1.5	o CH b
709				709		710	11 AU	726	0.3	710	12 AU	727	0.4	o Cβ′H b
		727		733	727									3 BU + 3 AG
749		753	752	750			12 AU	765	46.2	755	13 AU	778	76.2	o CH b
			776	775	775					776				5 BU + 1 AG
784		784	788	786			13 AU	796	0.6	784	14 AU	797	1.1	o CH b
814		815	815	814	814		14 AU	834	107.2	814	15 AU	836	155.2	o *meso*-CH b
			822s		818s		7 BU	836	0.9		7 BU	830	1.8	i *meso*-CH rock
889		892	884				15 AU	895	0.6		16 AU	895	0.5	o CβH Cβ′H b
878	880	879	879	878	878		8 BU	896	5.8	872	8 BU	890	9.7	i skel def
896			891				16 AU	905	3.5		17 AU	905	2.7	o CβH Cβ′H b
913	913	912	912	913	911		9 BU	947	181.3	891	9 BU	920	84.4	i NH Cβ′H def
							17 AU	957	0		18 AU	957	0	o *meso*-CH b
935	934	934	937	936	935		10 BU	965	193.7	917	10 BU	949	168.6	i skel def
944	sh													4 BU + 5 AG
964	967	975	970	971	971		18 AU	999	137.2	682	11 AU	720	0	NH as oop b
											11 BU	1012	76.4	i ND b skel def
987			991	991	992		11 BU	1028	5.6					i CH b
										984	12 BU	1041	43.7	i ND b skel def
			1002	1002	1003									13 AU + 4 BG
														5 AU + 9 BG
1026			1026	1025	1029									6 AU + 10 BG
1045	1041	1041	1045	1041	1042		12 BU	1075	96	1041	13 BU	1079	96.1	i im CH b
1059	1056	1055	1059	1055	1056		13 BU	1087	112.4	1057	14 BU	1089	164.5	i ph CH b
1089	1087	1086	1089	1090	1090		14 BU	1122	35.9					i CβH Cβ′H b
1166	1163	1163	1166	1166	1166		15 BU	1210	78.1	1167	16 BU	1209	60.5	i C10H C20H b
1188	1189	1188	1190	1189	1189		16 BU	1227	5.9	1195	17 BU	1229	7.9	i C9H C19H b
1223	1223	1222	1224	1224	1223		17 BU	1270	134.3					i NH CβH C10H C20H b
										1204				14 BU + 1 AG
1246	1246	1246	1250	1248	1247		18 BU	1285	107.4	1240	18 BU	1284	130.2	i C9H C19H ph Cβ′H b
										1255	19 BU	1296	56.4	i C10H C20H b skel def
1288	1288	1285	1290	1288	1288	1288	19 BU	1329	28.1	1290	20 BU	1326	37.2	i skel def C10H C20H b

Table 1 (*continued*)

Pc-d_0										Pc-d_2				
Observed[a]							Calculated[b]			Observed	Calculated			Assignment[d]
KBr	CCl_4	CS_2	Solid PC[c]	N_2	Xe	INS[c]	Symm	$\tilde{\nu}$	Int	KBr	Symm	$\tilde{\nu}$	Int	
										1325				12 BU + 3 AG
	1293	1291	1290	1296	1297	1296	20 BU	1336	23.8	1137	15 BU	1174	32.8	i NH ph CβH b
1355	1356	1356	1356	1355	1354		21 BU	1402	23.9	1343	21 BU	1386	86.1	i im CβH Cβ′H b
										1349				16 BU + 2 AG
1368	1369	1367	1368	1368	1368		22 BU	1411	41.3	1363	22 BU	1408	62.6	i *meso*-CH ph CβH Cβ′H b
1385	1382	1382			1379									12 BU + 3 AG
1406	1412	1407	1408	1409	1409		23 BU	1460	47.7	1384	23 BU	1432	64.3	i C9H C19H b
										1418	24 BU	1470	9.3	i C10H C20H b skel def
			1432	1433	1431		24 BU	1509	85.8		25 BU	1506	67.4	i C9H C19H b skel def
1458	1460		1456	1458	1458		25 BU	1516	75.5					i NH b skel def
1466	1467		1470	1469	1464		26 BU	1531	16	1466	26 BU	1522	79.5	i NH b skel def
1511			1512	1513	1513		27 BU	1571	61.8	1511	27 BU	1567	76.5	i skel def
1555			1560	1558	1556		28 BU	1617	152.6	1573	29 BU	1623	39.9	i NH b skel def
1572			1572	1573	1574		29 BU	1631	32.6	1546	28 BU	1593	67.2	i NH b skel def
					1604									18 BU + 4 AG
1631	1633	1629	1640							1642				19 BU + 3 AG
										1668				27 BU + 1 AG
1653		1657												13 BU + 6 AG
														19 BU + 4 AG
	1687	1686												5 BU + 14 AG
														14 BU + 6 AG
														27 BU + 2 AG
										1710				14 BU + 7 AG
														19 BU + 5 AG
														21 BU + 4 AG
										1778				6 BU + 16 AG
														12 BU + 8 AG
1778	1779	1775	1785	1772										5 BU + 16 AG
														16 BU + 6 AG
1876	1875	1873	1887	1885										9 BU + 10 AG
										1943				11 BU + 12 AG
														29 BU + 4 AG
										1974				10 BU + 14 AG
	2444	2444		2446		2422								12 BU + 23 AG
														18 BU + 17 AG
														19 BU + 16 AG
														24 BU + 12 AG
	2543	2542		2540		2514								12 BU + 27 AG
														28 BU + 12 AG
														29 BU + 10 AG
		2617		2620										13 BU + 29 AG
														16 BU + 25 AG
														17 BU + 23 AG
														18 BU + 22 AG
														21 BU + 19 AG

Table 1 *(continued)*

Pc-d_0									Pc-d_2				
Observed[a]							Calculated[b]			Observed	Calculated		Assignment[d]
KBr	CCl_4	CS_2	Solid PC[c]	N_2	Xe	INS[c]	Symm	$\tilde{\nu}$	Int	KBr	Symm	$\tilde{\nu}$	Int	
		2642		2642										12 BU + 30 AG
							30 BU	2895	433.9		30 BU	2157	252.4	14 BU + 29 AG
3020	3027	3029	3020	3021	3021		31 BU	3165	13	3012	31 BU	3165	13.3	18 BU + 23 AG
3051	3064	3065	3056	3047			32 BU	3184	53.4	3058	32 BU	3184	53.5	as i NH str
3076	3090	3089	3079	3080	3085		33 BU	3236	8.3	3079	33 BU	3236	8.2	*meso*-CH str
			3087				34 BU	3250	2.6	3079s	34 BU	3250	2.6	ph CβH Cβ′H str
3092	3110	3108	3098	3099			35 BU	3256	31.1	3097	35 BU	3256	31.4	im CβH Cβ′H str
3113			3115	3114			36 BU	3268	18.3	3114	36 BU	3268	18.6	ph CβH Cβ′H str
3127s										3133s				im CβH Cβ′H str
														29 BU + 29 AG

[a] cm^{-1}. [b] B3LYP/6-31G(d,p), intensity in km mol^{-1}, no scaling factor applied. [c] 10 K. [d] Abbreviations: s, symmetric; as, antisymmetric; str, stretch; b, bend; i, in-plane; o, out-of-plane; skel def, skeletal deformation; im, diimine; ph, phenylene; bp, bipyridyl.

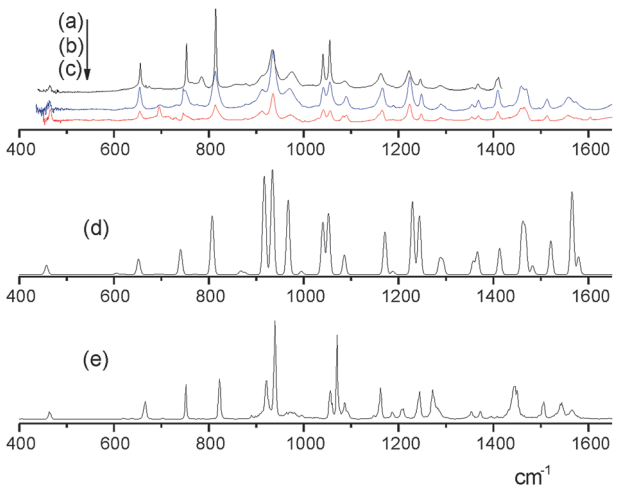

Fig. 1 IR spectra of Pc-d_0: experimentally recorded absorption for CS_2 solution at 293 K (a), N_2 matrix at 10 K (b), and Xe matrix at 9 K (c); harmonic DFT calculations using B3LYP/6-31G(d,p) assuming Gaussian peaks of 4 cm^{-1} halfwidths for all transitions and a scaling factor of 0.968 (d); *ab initio* molecular dynamics simulations at 300 K using BLYP/PW with the scaling factor of 1.032 (e).

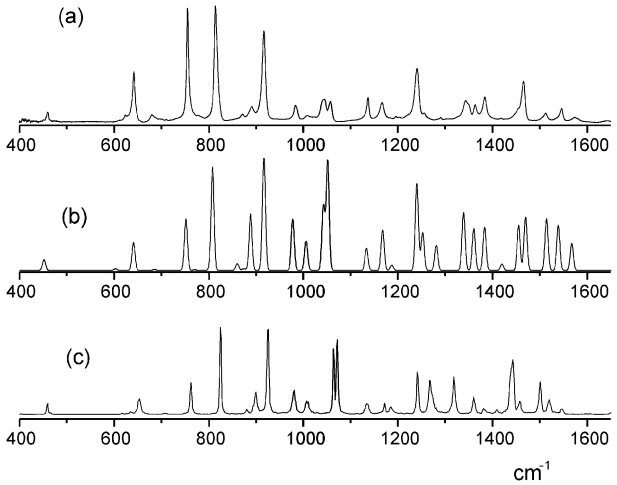

Fig. 2 IR spectra of Pc-d_2: experimentally measured absorption in a KBr pellet at 293 K (a); harmonic DFT calculations using B3LYP/6-31G(d,p) assuming Gaussian peaks of 4 cm^{-1} halfwidths for all transitions with the scaling factor of 0.966 (b); *ab initio* molecular dynamics simulations at 300 K using BLYP/PW with the scaling factor of 1.032 (c).

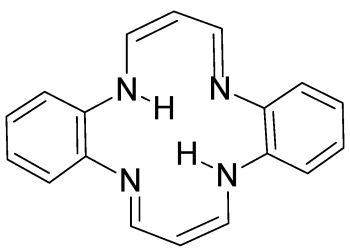

Scheme 3 Dibenzo[*b*,*i*][1,4,8,11]tetraaza[14]annulene (TAA).

BU vibrations. In Tables 1 and 2 we placed in separate rows modes coming from the isotopologues for which no obvious 1 : 1 correlation could be found between their vibrational forms.

Table 2 Observed and computed modes of *gerade* symmetry

Pc-d_0													Pc-d_2							
Observed[a]									Calculated[b]				Observed				Calculated			Assignment[i]
Raman					Fluorescence				INS[h]				Raman			Flu				
Solid Pc	Acetone	CCl_4	N_2[c]	Xe[c]	Ar[d]	N_2[e]	jet[f]	He[g]		Symm	$\tilde{\nu}$	Int	Solid Pc	Acetone	CCl_4	He	Symm	$\tilde{\nu}$	Int	
120s									120	1 BG	119	0.5	120s				1 BG	119	0.5	o tilt
					146	147	147		134	2 BG	137	5.3	144				2 BG	136	5.3	o tilt
149	145	152	150	150	158			145	150	1 AG	150	31.2	153			142	1 AG	150	31	i tilt
180s	181		182	181	181	184	178	181	178	2 AG	187	23.6	182	184		184	2 AG	185	22.8	i rock
										3 BG	198	1.3					3 BG	198	1.5	o tilt
219			220	222	221				226	4 BG	209	7.3	220				4 BG	208	7	o *meso*-CH b
			320	320				324								326				1 AG + 2 AG
																331				1 AG + 3 BG
341	342		342	342	344	344	341	343		3 AG	347	75	339	340		337	3 AG	345	74.4	i im ph rock
365	366		367	366	370	362	364	367	370	4 AG	370	41.4	365	366		364	4 AG	370	40.4	i CβH Cβ′H b
				380																3 BG + 3 BG
397			399	399						5 BG	399	0.7	399				5 BG	398	0.7	o CβH Cβ′H b
480			482	482		487	481	483	485	5 AG	491	0.2	477	479		476	5 AG	487	0.4	i im ph rock
			505	505						6 BG	493	0.1					6 BG	493	0.1	o *meso*-CH CβH b
						524	520									521				2 AG + 3 AG
						535	542									549				2 AG + 4 AG
594			591	591				599		6 AG	610	5.6	591	590		596	6 AG	608	6.2	i skel def
614				625						7 BG	644	1.8	610				8 BG	645	1.3	o Cβ′H b
633													635							1 AG + 5 AG
648s				646						8 BG	673	10.2	664s				9 BG	696	6.5	o *meso*-CH CβH b
664	665	665	667	664	669	668	667	668	670	7 AG	674	23.2	656	655	655	654	7 AG	666	22.3	i skel def
						683	682									675				3 AG + 3 AG
697			699	700		698	705			9 BG	713	1.4	687				10 BG	713	1.6	o CβH Cβ′H b
	706		712	712					710	10 BG	718	1.3	699	708			11 BG	720	1.9	o CβH Cβ′H b
						735		732												
			766s	767						11 BG	775	3.6	770s				12 BG	781	5.5	o CH b
798s				786s				790		12 BG	789	10.5					13 BG	792	7.9	o CH b
			825s	823s				825		13 BG	832	5.4	821s				14 BG	835	5.6	o *meso*-CH Cβ′H b
810			811	810						8 AG	833	2.2	797				8 AG	823	7.6	i skel def
859			859	855		859		863		9 AG	877	6.7	852	853	854	855	9 AG	870	9.8	i skel def
877				877						14 BG	897	0.4					15 BG	897	0.3	o ph CβH Cβ′H b
892										15 BG	904	0.3	892				16 BG	904	0.3	o im CβH Cβ′H b
			904s	900						16 BG	933	0.4	623				7 BG	641	4.4	o NH b
940s			940s	936		927				17 BG	958	3.8					17 BG	958	3.9	o *meso*-CH b
967	965		966	963	966	961	966	964		10 AG	989	81.4	956		960	957	11 AG	982	70.4	i skel def
			972	970				970		11 AG	994	23	925	928	927	928	10 AG	957	46.5	i skel def
													965							5 AG + 5 AG
988	990	969	993	990	996		990	995		12 AG	1016	84.5	983	986	986	989	12 AG	1011	74.7	i skel def
1004		1003				1006							1007							3 AG + 7 AG
																1021	13 AG	1055	0.3	i NH CβH Cβ′H b

Table 2 (*continued*)

Pc-d_0													Pc-d_2							
Observed[a]										Calculated[b]			Observed				Calculated			Assignment[i]
Raman					Fluorescence				INS[h]				Raman			Flu				
Solid Pc	Acetone	CCl_4	N_2[c]	Xe[c]	Ar[d]	N_2[e]	jet[f]	He[g]		Symm	$\tilde{\nu}$	Int	Solid Pc	Acetone	CCl_4	He	Symm	$\tilde{\nu}$	Int	
1048			1054	1050				1053		13 AG	1083	10.3		1066		1067	15 AG	1099	23.6	i CβH Cβ′H b
1060	1066	1060	1062	1061	1065	1063	1060	1064		14 AG	1092	84.9	1059		1060	1061	14 AG	1091	79.2	i CβH Cβ′H b
1116	1117	1114	1116	1115	1119	1110		1118		15 AG	1142	6.8	1135			1137	16 AG	1165	3.8	i CβH Cβ′H b skel def
1160	1160	1159	1159	1159	1163	1161	1160	1161		16 AG	1193	22.6	1165	1171	1168	1169	17 AG	1203	45	i skel def
1198	1202	1199	1200	1199	1205	1204	1202	1206	1204	17 AG	1240	107.9	1198	1202	1201	1203	18 AG	1240	141.6	i *meso*-CH b skel def
													1228	1231	1230					4 BG + 13 AG
		1251	1251	1249	1252			1255		18 AG	1292	86.9	1257	1259	1261	1261	19 AG	1298	119.5	i skel def
													1275		1278					5 AG + 8 AG
1258	1259	1264	1264	1262	1267	1258	1260	1265		19 AG	1312	236.6								i skel def NH b
													1312		1314	1317	20 AG	1355	83.9	i skel def NH b
1327	1339	1330		1331	1333	1336	1336	1336		20 AG	1370	225.2	1326		1330	1333	21 AG	1371	236.2	i ph CβH Cβ′H b
1339	1343s		1342	1342				1348		21 AG	1387	13.9	1358		1354	1355	22 AG	1400	51.2	i NH b skel def
1367	1369	1376	1375	1372	1384			1382		22 AG	1413	56.6	1375		1379	1382	23 AG	1416	26.3	i im CβH Cβ′H b skel def
																1397	24 AG	1446	71	i skel def C9H C19H b
1393	1396	1399	1398	1398	1395	1398	1403	1404		23 AG	1442	205.8								i skel def C9H C19H b
													1399		1404	1408	25 AG	1456	117.6	i skel def
			1408					1413		24 AG	1448	27.8								i skel def
1427	1424	1431	1428					1430	1435	25 AG	1489	514								i NH b skel def
1465	1470	1478		1471		1472	1478	1472		26 AG	1532	118.2	1459		1466	1468	26 AG	1517	704.1	i NH b skel def
1495	1497	1495		1494	1507	1511	1506	1507		27 AG	1563	341.6	1492		1495	1502	27 AG	1552	287.1	i NH b skel def
1540	1540	1543	1542	1542				1550		28 AG	1592	567.1	1538		1540	1542	28 AG	1591	683.8	i skel def
1555	1559	1561	1563	1562	1559	1568	1567	1567		29 AG	1613	905.5	1553		1559	1561	29 AG	1609	696.3	i skel def
1606	1607	1608	1609	1608	1606	1609	1615	1620		30 AG	1663	440.5	1592		1595	1600	30 AG	1632	590.1	i NH b skel def
1632s																				7 AG + 10 AG
1874													1876							3 AG + 28 AG
										31 AG	2895	4.7					31 AG	2156	3.9	i s NH b
3093										32 AG	3165	102.1	3092				32AG	3165	102	*meso*-CH s
3125			3120	3126					3123	33 AG	3184	745.3					33AG	3184	745.3	*meso*-CH s
3157										34 AG	3236	266.9					34 AG	3236	266.9	ph CβH Cβ′H s
			3164							35 AG	3250	266.7					35 AG	3250	266.8	im CβH Cβ′H s
3176										36 AG	3256	498					36 AG	3256	497.6	ph CβH Cβ′H s
			3209							37 AG	3268	617.4					37 AG	3268	617.5	im CβH Cβ′H s

[a] cm^{-1}, $T = 293$ K unless noted otherwise. [b] B3LYP/6-31G(d,p), Raman scattering activity in $Å^4$ amu^{-1}, no scaling factor applied. [c] Nitrogen and xenon matrices,10 K. [d] Fluorescence in argon matrix, ref. 10. [e] Fluorescence in nitrogen matrix, ref. 68. [f] Fluorescence in supersonic jet, ref. 31. [g] He droplets, $T = 0.37$ K. [h] $T = 10$ K. [i] Abbreviations as in Table 1.

3.2 Modes of gerade symmetry

The assignments of vibrations belonging to *gerade* symmetry species seem even more reliable than those for IR-active modes, because the available experimental database is much larger. The AG and BG vibrations are observed not only in the Raman spectra, but also in fluorescence. Moreover, using different wavelengths for Raman excitation, we were able to switch from a non-resonant to a resonant regime, the latter probing different electronic states. In addition, analysis of depolarization enabled distinguishing between AG and BG modes. Finally, some experiments, to be discussed elsewhere in detail, involved SERS or SERRS measurements. Therefore, multiple cross-checks were possible, yielding essentially the same transition energies, but the intensity of different bands responding differently to changes under the conditions of Raman measurements. Finally, as in the case of IR-active transitions, additional support was provided by the INS spectra.

The fluorescence spectrum of Pc-d_0 embedded in liquid He droplets (Fig. 3) consists of doublets, which are due to tunneling splitting caused by the quantum delocalization of the internal hydrogens. The splittings are no longer resolved for Pc-d_2. The spectra are dominated by totally symmetric modes. Thirty AG modes are predicted in the range below 1700 cm^{-1}. All but one could be assigned in the fluorescence spectra for both Pc-d_0 and Pc-d_2. The only missing mode, 8 AG, could, however, be readily identified in the Raman spectra, due to its characteristic red shift of 13 cm^{-1} upon deuteration.

Inspection of Fig. 3 shows that both positions and relative intensities of vibronic components, including overtones and combinations, are nicely predicted by calculations. Only for one mode, 14 AG, the computed intensity is considerably lower than the observed ones in both parent and deuterated compounds, even though its location is predicted accurately.

The Raman spectra are shown in Fig. 4 and 5. Most importantly, they not only confirm the assignments of the AG modes, but also provide the positions of the BG modes, which were practically absent in fluorescence. Comparison of spectra obtained with different laser lines, corresponding to both nonresonant (785 nm) and resonant regimes (325 and 514 nm), reveals some, but not dramatic, changes in the relative intensities. Some variations in relative intensities are also observed for different environments. In general, the largest intensities in the Raman spectra are observed for totally symmetric AG modes. Analogous situation was reported for Raman spectra of porphyrin obtained for nonresonant excitation; it was explained as indication of the dominance of Franck–Condon over Herzberg–Teller mechanism.[58]

It should be noted that the Raman activities of vibrational modes computed by such software packages as Gaussian are not directly related to the experimental spectrum. A proper comparison requires taking into account the laser frequency and that of a particular vibration, as well as the Boltzmann factor, responsible for the temperature dependence. Such a procedure was applied in this work. As shown in Fig. 4 and 5, the simulated Raman spectra reproduce the experimental pattern quite accurately for both Pc-d_0 and Pc-d_2.

On the basis of combined Raman, fluorescence, INS measurements, analysis of isotopic shifts and theoretical studies, we propose the assignments for thirty six out of thirty seven AG modes and for all BG species (Table 2). As was the case for the IR-active modes, we could not observe the vibration corresponding to the N–H stretch, 31 AG. The 3 BG mode was only identified as an overtone and in combination with 1 AG.

Correlation between the experimental and calculated transitions yielded the RMS errors of 7 cm^{-1} for Pc-d_0 and 10 cm^{-1} for Pc-d_2. As was the case for *ungerade* species, very similar results were obtained using the 6-31G(d,p) and 6-311++G(fd,2dp) basis sets. Again, somewhat larger scaling factors were obtained for the latter, 0.972 for Pc-d_0 and 0.973 for Pc-d_2, compared with 0.966 obtained for both isotopologues while using 6-31G(d,p).

Regarding vibrations related to the intramolecular hydrogen bonds, the theory predicts very small intensities for both N–H stretching and out-of-plane bending bands. However, we were able to identify the out-of-plane bending mode, 16 BG, which shifts to the red after deuteration by approximately 280 cm^{-1}, the same amount as the corresponding IR-active 18 AU counterpart. Interestingly, the spectral pattern observed after deuteration in the 1100–1600 cm^{-1} region is not so strongly modified as was the case for the IR spectra.

3.3 Theoretical modeling and interpretation of the IR spectra

The patterns of IR spectra of Pc-d_0 and Pc-d_2, computed from *ab initio* molecular dynamics (AIMD) trajectories generated at the BLYP/PW level, compare well with the experimental data in the near infrared region (*cf.* the top and bottom panels in Fig. 1 and 2). The band locations below 1600 cm^{-1} are predicted with similar accuracy to those obtained from the static normal mode analysis (NMA) using B3LYP/6-31G(d,p) within harmonic approximation, and the intensity patterns are even better. This reassuring observation provides a premise for applying the AIMD method as a tool to explore the discrepancy between experimental and theoretical results for the N–H stretching vibration, where static calculations obviously break down (see Section 3.1). In the following section we confront anharmonic frequencies ν_i of the IR bands computed from the AIMD trajectories (see Section 2 for the definition of the anharmonic frequencies ν_i) with the experimentally measured values and analyze the underlying molecular motions in order to explain the intriguing features of the IR spectra of porphycene in the high frequency region.

The correction factors, calculated independently for the two isotopologues, Pc-d_0 and Pc-d_2, yield $c_{d_0} = 1.0318$ and $c_{d_2} = 1.0320$, respectively. Since the experimental data for singly deuterated species, Pc-d_1, are not available and the difference between c_{d_0} and c_{d_2} is rather small, we applied one common correction factor $c = 1.032$ to all three sets of frequencies, including the one obtained for Pc-d_1. The correction magnitude for the dynamical BLYP/PW calculations and for the harmonic B3LYP/6-31G(d,p) ones is similar. However, the anharmonic BLYP model appears to provide a "softer" potential than that of the actual molecule ($c > 1$), while the potential in the harmonic B3LYP model seems to be too stiff ($c < 1$). Similar difference between two DFT models has been observed before.[67] The anharmonic frequencies match the experimental ones with the 15 cm^{-1} standard deviation (an average over Pc-d_0 and Pc-d_2 data sets). We conclude that the theoretical

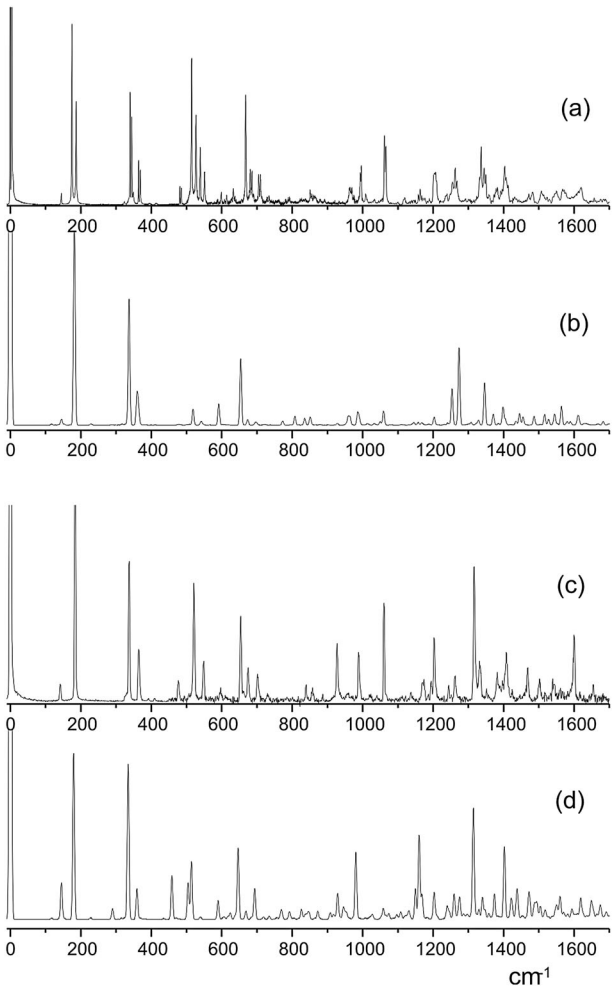

Fig. 3 Dispersed fluorescence of Pc-d_0 (a) and Pc-d_2 (c) in helium droplets along with the simulated spectra (b and d).

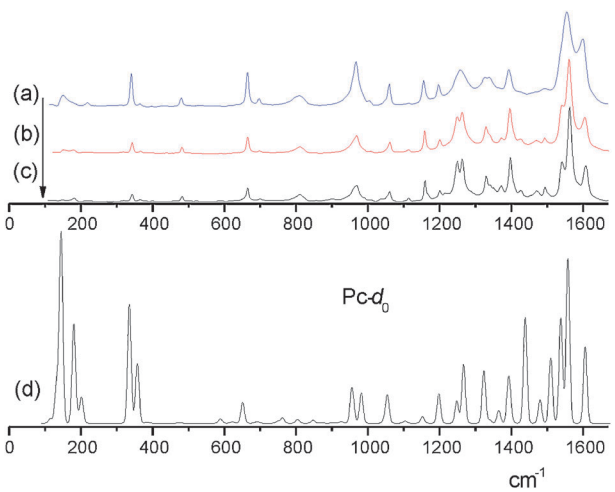

Fig. 4 Top, experimental Raman spectra of Pc-d_0 obtained with 514 nm laser line: (a) polycrystalline Pc, 293 K; (b) nitrogen matrix, 10 K; (c) xenon matrix, 10 K; (d) the spectra simulated carrying out B3LYP/6-31G(d,p) calculations, corrected for the laser wavelength and for the temperature of 290 K. Gaussian peaks of 6 cm^{-1} halfwidths were assumed for all transitions. The scaling factor of 0.966 was used.

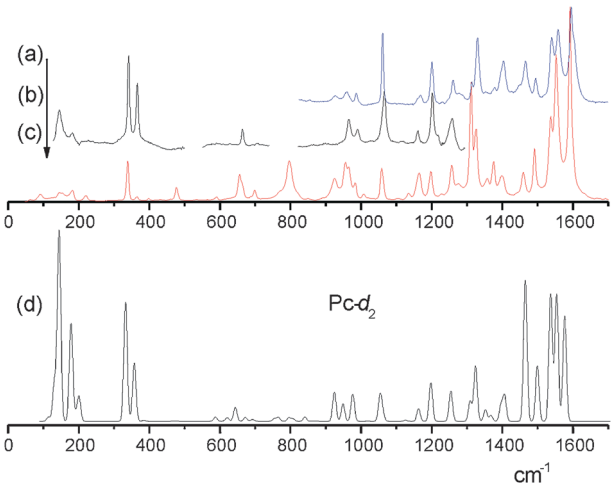

Fig. 5 Top, experimental Raman spectra of Pc-d_2 at 293 K obtained with 514 (a and c) or 785 nm (b) laser lines: (a) CCl_4; (b) acetone; (c) polycrystalline sample; (d) the spectra simulated carrying out B3LYP/6-31G(d,p) calculations, corrected for 785 nm laser wavelength and for the temperature of 290 K. Gaussian peaks of 6 cm^{-1} halfwidths were assumed for all transitions. The scaling factor of 0.966 was used.

predictions of the IR spectra based on dynamical *ab initio* calculations are accurate and agree with the experimental measurements within an acceptable error limit.

Crucial for the purpose of the present work are the results obtained for the high-energy range of the IR spectrum (see the bottom panel and horizontal axis in Fig. 6). For the sake of simplicity, in the following discussion we will omit the scaling factors and will refer to the raw frequency values, both harmonic and anharmonic, as obtained from the BLYP/PW computations. Two distinguished features centered at 3100 and 3170 cm^{-1} result

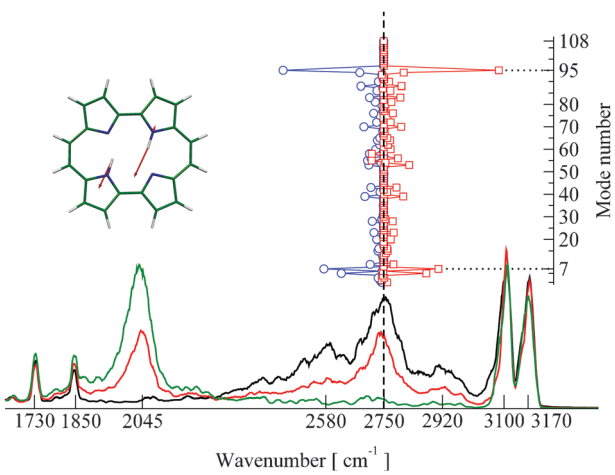

Fig. 6 Computed high frequency range of the IR spectrum of Pc-d_0 (black line), Pc-d_1 (red line) and Pc-d_2 (green line). Harmonic frequency f_{96} = 2753 cm^{-1} of the asymmetric N–H stretching mode 30 BU (vertical dashed line), perturbed frequencies $f_{96,j}^{-}$ (blue circles) and $f_{96,j}^{+}$ (red squares) of the 30 BU mode as defined in the text, as a function of a perturbing mode number j (vertical right panel); displacement vector of the asymmetric N–H stretching mode 30 BU subject to perturbations from other vibrational modes (left panel). All calculations were carried out using the BLYP/PW exchange-correlation functional, no scaling factor for the frequencies was applied.

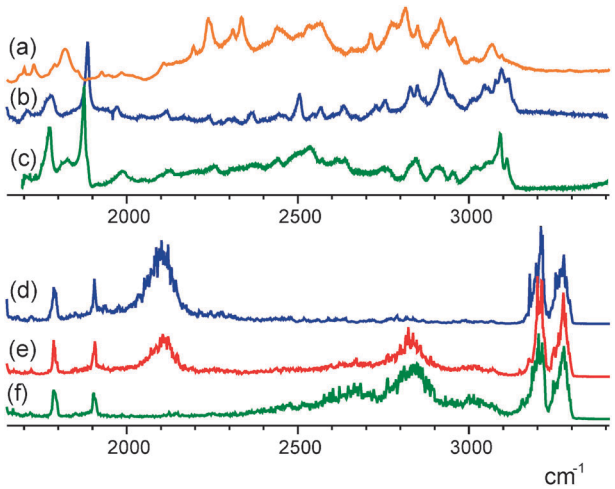

Fig. 7 Top, the experimental IR spectrum recorded at 293 K for Pc-d_{12} (a), Pc-d_2 (b) and Pc-d_0 (c) in KBr. Bottom, IR spectrum of Pc-d_2 (d), Pc-d_1 (e) and Pc-d_0 (f) in the high frequency range as calculated from *ab initio* molecular dynamics simulations using the BLYP/PW exchange-correlation functional.

from the C–H stretching vibrations, with the lower frequency corresponding to the *meso* C–H bonds. As expected, both spectral features due to C–H stretches remain unaffected upon deuteration of the two internal hydrogens. This is not only the argument for the correct assignment of the modes, but it also provides an evidence for the motions of the inner hydrogens being decoupled from those of the peripheral ones.

Another two theoretical peaks are located around 1730 and 1850 cm^{-1}. Their positions are not shifted upon deuteration of the internal hydrogen sites. Upon closer inspection each of the two features appears to be composed of two close-lying signals separated by approximately 7 cm^{-1}. The lack of respective counterparts in the harmonic calculations (both B3LYP/6-31G(d,p) and BLYP/PW) indicates that these signals are due to combinations or overtones of fundamental vibrational modes. Indeed, excellent agreement is observed between the theoretical and experimental bands for both, Pc-d_0 and Pc-d_2 (see Fig. 7).

The positions and intensities of the bands in the infrared region of the spectrum that extends roughly between 1900 and 3000 cm^{-1} depend on the mass of the inner hydrogen atoms. In the undeuterated species, Pc-d_0, a broad feature extends over the range of about 750 cm^{-1} and consists of one main peak centered around 2750 cm^{-1} and two shoulders—both separated by about 170 cm^{-1} from the main peak. In singly deuterated species, Pc-d_1, the integral intensity of this feature is two times smaller than in Pc-d_0 and a new feature appears around 2045 cm^{-1}, red-shifted by about 700 cm^{-1} from the main frequency of the first peak. In Pc-d_2, the high-energy peak fully disappears, while the feature at 2045 cm^{-1} becomes roughly two times more intense than in Pc-d_1. This characteristic isotope effect provides evidence that the bands observed in this spectral region result from the motions of the two hydrogen atoms involved in the internal N–H···N hydrogen bonds.

As already mentioned, porphycene has 108 internal degrees of freedom (DOF). In the vicinity of the potential energy minimum they can be approximated by the eigenvectors of the Hessian matrix, representing normal vibrational modes (NM). In porphycene this harmonic model describes the majority of DOFs quite well. This is reflected by the fact that most of the projected normal mode (PNM) power spectra, $p_i(\omega)$, contain single, highly intense peaks, lying close to the corresponding normal mode eigenvalues, f_i. Due to anharmonicity of the realistic DFT-based potential used for generating the molecular dynamics trajectories, the positions of the peaks are shifted with respect to their harmonic counterparts. The shift amounts to $\sim$10 cm^{-1} on average, usually towards lower frequencies (red-shift). Only in two cases, *i.e.* for modes $\boldsymbol{e}_5$ and $\boldsymbol{e}_{13}$ assigned to 1 AG and 2 BU vibrations, respectively, a blue shift of a few wavenumbers was observed (see ESI† for the corresponding displacement vectors). In some cases the power spectra contain additional, less intense peaks, mainly in the low frequency region. The additional frequencies in the PNM spectra are either due to numerical noise, *e.g.*, normal mode vectors being not perfectly orthogonal or the inter-mode interactions (see Section 3.4 for details).

There are only two exceptions from the single-peaked shape of the PNM spectra of the undeuterated Pc-d_0 species: these are modes $\boldsymbol{e}_{95}$ and $\boldsymbol{e}_{96}$ which show extremely broad features in the high frequency region that closely resemble the already-mentioned band at 2750 cm^{-1} in the IR spectrum. The underlying molecular motions of the two modes consist of the N–H bond stretching vibrations. The lower $\boldsymbol{e}_{95}$ frequency mode corresponds to simultaneous elongation and shortening of the two bonds (in phase, also termed symmetric stretch), while in the higher $\boldsymbol{e}_{96}$ frequency mode one bond gets shortened while the other gets elongated at the same time (in counter-phase, asymmetric stretch). The two BLYP/PW modes correspond to 31 AG and 30 BU vibrations calculated using the harmonic B3LYP/6-31G(d,p) model, with the latter representing the IR active vibration which, unexpectedly, has not been identified in the experimental spectrum (we should note that the excitation of the symmetric 31 AG mode is likely to enhance the concerted proton transfer reaction mechanism, while excitation of the asymmetric 30 BU vibration is expected to drive the stepwise reaction). To shortly summarize the results: so far, PNM-based analysis allowed us to assign the relevant features in the IR spectrum to the specific atomic motions, however, it did not provide insight into their interactions with the other modes that would explain the extreme broadening of the N–H stretching band. Inter-mode couplings are discussed in the following paragraph.

3.4 Inter-mode couplings and broadening of the N–H stretching vibration

In realistic molecular systems the internal degrees of freedom are, in general, interdependent. Deformation of the molecular structure along one DOF is likely to modify the potential energy function in all remaining internal degrees of freedom. Such perturbation would give rise to the force acting on the system along the unperturbed degrees of freedom. Analysis based on this observation has been performed for porphycene using a limited number of modes.[35,36] Consequently the perturbation of the PES along one normal mode vector would affect the force constants, and thus vibrational frequencies

associated with the remaining normal modes. In the following we apply the quantitative approach that takes into account couplings of all normal modes to the asymmetric N–H stretching mode 30 BU in porphycene (see inset in Fig. 6 for the corresponding displacement vector), however, it can be easily generalized (see ESI† for the details of this method). In a nutshell, the harmonic frequency of the ith normal mode is perturbed by the displacement along another normal mode j. The perturbation is quantified by two limiting values f_{ij}^{+} and f_{ij}^{-} resulting from the displacement in the positive and negative directions along the modulating mode j. The magnitude of the perturbation reflects the average amplitude of fluctuations along j at a given temperature.

Normal modes of vibration can be categorized into fast- and slow-varying degrees of freedom, based on their corresponding frequencies. The slow modes are characterized by relatively small curvature of the PES as compared to the fast ones, though the distinction between the two is somewhat arbitrary at this point. As an example, one may consider the slowest normal mode of Pc-d_0 – $\boldsymbol{e}_1$ with eigenfrequency $f_1 = 86$ cm^{-1} which has a period of oscillations $T \approx 400$ fs, while the fastest one, $\boldsymbol{e}_{108}$ ($f_{108} = 3198$ cm^{-1}) varies on the time scale of $\sim$10 fs. Within one vibrational period along the slow DOF the system performs several tens of oscillations along the fast one. As already mentioned, the shape of the PES along the fast mode may depend on the instantaneous displacement along the slow mode. For such a case, the motion along the j, the slow DOF modulates the frequency of oscillations along the fast mode i, which then becomes a function of the displacement $f_i(d_j)$.

Such frequency modulation is indeed observed in porphycene at 300 K. The harmonic frequency of the IR active N–H stretching mode 30 BU is significantly perturbed by the coupling to other modes (see vertical panel in Fig. 6 for perturbed frequencies $f_{96,j}^{+}$ and $f_{96,j}^{-}$ of the mode 30 BU in Pc-d_0 species as a function of the perturbing mode number j). The largest perturbation results from the fluctuations along $\boldsymbol{e}_{95}$ ($j = 95$)—the infrared inactive mode 31 AG (see Fig. 8 for the displacement vectors of all relevant normal modes discussed in this section) which modulates the value of f_{96} in the range between 2455 and 3085 cm^{-1}, spanning 630 cm^{-1} and being sensitive to the inner H/D substitution. It should be pointed out that the normal frequencies of both, the perturbed mode 30 BU and the perturbing mode 31 AG, are only few wavenumbers apart and therefore they cannot be considered fast and slow with respect to each other. It implies that the simple concept of frequency modulation may not be fully appropriate to explain the mechanism of the inter-mode interaction in this case. However, the existence of such interaction is undeniable.

There are two other modes that introduce significant perturbation to f_{96}. The normal mode 2 AG ($j = 7$), widely discussed[18,27,35,36] in the context of the mechanism of the double proton transfer reaction in porphycene, modulates the fundamental frequency of the 30 BU mode within the range of 334 cm^{-1}, between 2575 cm^{-1} and 2910 cm^{-1}. Interestingly the shoulders associated with the main N–H signal discussed in Section 3.3 lie precisely on the boundaries of this range (*cf.* black curve in the horizontal panel and open symbols in the vertical panel of Fig. 6). Perturbation of f_{96} due to the mode 1 AG ($j = 5$) is enclosed within 2625 and

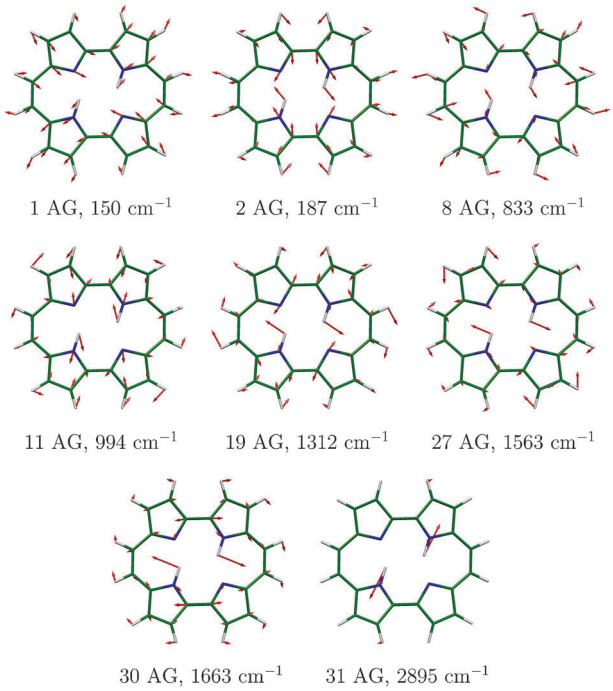

Fig. 8 Displacement vectors of the normal modes in Pc-d_0 relevant to the broadening of the asymmetric N–H stretching mode 30 BU, as obtained with B3LYP/6-31G(d,p).

2873 cm^{-1}—spanning the range of 248 cm^{-1}. Other five normal modes, 8 AG ($j = 39$), 11 AG ($j = 53$), 19 AG ($j = 70$), 27 AG ($j = 88$), and 30 AG ($j = 94$), contribute more than 100 cm^{-1} to the broadening of the f_{96} peak. The majority of all modes, *i.e.* 74 out of 108, do not couple to the mode 30 BU since the broadening of the fundamental frequency f_{96} due to the activation of those modes is smaller than 10 cm^{-1}. In conclusion, the low, if not undetectable, intensity of the N–H stretching vibration in the experimental IR spectra results from the broadening caused by other modes. Coupling of the asymmetric 30 BU mode to the low frequency 7 AG mode was discussed previously by many authors[18,27,35,36] and our results confirm nicely their findings. The extended analysis presented here reveals other additional modes that contribute significantly to the broadening of the IR N–H stretching vibration (Fig. 8).

We close the discussion on inter-mode interactions with the remark that the results presented here were obtained from the full-dimensional PES obtained at the *ab initio* level and without making any assumption on its shape. The harmonic *ansatz* was invoked only to decompose the complex molecular motions into easy-to-visualize components, and to quantify the coupling effects.

4. Summary and conclusions

Using combined experimental and theoretical procedures resulted in the assignments of 105 out of 108 vibrations of porphycene. DFT seems, especially when combined with isotopic substitution, to be a good method for a reliable analysis of vibrational structure. However, it is clear that the analysis of strong hydrogen bonds requires a special treatment.

The results of theoretical analysis, which goes beyond the harmonic approximation, allowed the interpretation of the IR spectra. We postulate that the apparent lack of the N–H stretching band in the experimental spectra, predicted by harmonic calculations to be the strongest in the IR spectrum, is caused by its extreme breadth. The integrated intensity is very high, but the height at maximum is not. The large spectral width is due to the interaction of the N–H stretch with other modes, in particular those which alter the N···N distance, and thus the HB strength. One can envisage the frequency of the N–H stretch as being continuously modulated by the low frequency modes.

The unequivocal experimental confirmation of this model may not be easy. The experimental IR spectra (Fig. 7) clearly show an extremely broad band in the range of 2000–3000 cm^{-1}, with many structured features superimposed upon the underlying continuum. The maximum of the broad band lies around 2500 cm^{-1}, about 200 cm^{-1} lower than predicted by theory. An analogous broad feature has been observed for Pc-d_{12}, but not for Pc-d_2. Interestingly, for the latter theory predicts a much narrower band.

Our results may be relevant for the elucidation of the mechanism of double hydrogen transfer in porphycenes. The experiments performed for porphycenes isolated in the jet or embedded in helium droplets revealed tunneling splittings of which the values were strongly mode-dependent.[15,20,31] The present findings clearly indicate the multidimensional character of the internal hydrogens motions. Time-resolved vibrational spectroscopy experiments in the condensed phase are planned, with the goal of obtaining a detailed picture of intramolecular mode coupling.

Acknowledgements

We appreciate the help of Samantha Ford in neutron scattering experiments. ŁW is grateful to Harald Forbert for valuable discussions. The work was supported by the European Union within European Regional Development Fund, through the Innovative Economy grant (POIG.01.01.02-00-008/08) and by the Polish Ministry of Science and Higher Education (N N519 384736). The simulations were carried out at ICM University of Warsaw (Halo2), and in Forschungszentrum Jülich (Juropa). The INS experiments were supported by the Institut Laue-Langevin proposal 7-04-83.

Notes and references

1 *Handbook of Porphyrin Science*, ed. K. Smith, K. Kadish and R. Guilard, World Scientific, Singapore, 2010.
2 P. F. Aramendia, R. W. Redmond, S. Nonell, W. Schuster, S. E. Braslavsky, K. Schaffner and E. Vogel, *Photochem. Photobiol.*, 1986, **44**, 555–559.
3 J. Waluk, M. Müller, P. Swiderek, M. Köcher, E. Vogel, G. Hohlneicher and J. Michl, *J. Am. Chem. Soc.*, 1991, **113**, 5511–5527.
4 J. C. Stockert, M. Cañete, A. Juarranz, A. Villanueva, R. W. Horobin, J. Borrell, J. Teixidó and S. Nonell, *Curr. Med. Chem.*, 2007, **14**, 997–1026.
5 J. Braun, H. H. Limbach, P. G. Williams, H. Morimoto and D. E. Wemmer, *J. Am. Chem. Soc.*, 1996, **118**, 7231–7232.
6 J. Braun, M. Schlabach, B. Wehrle, M. Köcher, E. Vogel and H. H. Limbach, *J. Am. Chem. Soc.*, 1994, **116**, 6593–6604.
7 M. Schlabach, B. Wehrle, H. Rumpel, J. Braun, G. Scherer and H. H. Limbach, *Ber. Bunsen-Ges. Phys. Chem.*, 1992, **96**, 821–833.
8 B. Wehrle, H. H. Limbach, M. Köcher, O. Ermer and E. Vogel, *Angew. Chem., Int. Ed. Engl.*, 1987, **26**, 934–936.
9 P. M. Kozlowski, M. Z. Zgierski and J. Baker, *J. Chem. Phys.*, 1998, **109**, 5905–5913.
10 K. Malsch and G. Hohlneicher, *J. Phys. Chem. A*, 1997, **101**, 8409–8416.
11 J. Baker, P. M. Kozlowski, A. A. Jarzecki and P. Pulay, *Theor. Chem. Acc.*, 1997, **97**, 59–66.
12 H. Piwoński, C. Stupperich, A. Hartschuh, J. Sepioł, A. Meixner and J. Waluk, *J. Am. Chem. Soc.*, 2005, **127**, 5302–5303.
13 U. Langer, C. Hoelger, B. Wehrle, L. Latanowicz, E. Vogel and H. H. Limbach, *J. Phys. Org. Chem.*, 2000, **13**, 23–34.
14 M. Gil, J. Jasny, E. Vogel and J. Waluk, *Chem. Phys. Lett.*, 2000, **323**, 534–541.
15 J. Sepioł, Y. Stepanenko, A. Vdovin, A. Mordziński, E. Vogel and J. Waluk, *Chem. Phys. Lett.*, 1998, **296**, 549–556.
16 T. Yoshikawa, S. Sugawara, T. Takayanagi, M. Shiga and M. Tachikawa, *Chem. Phys. Lett.*, 2010, **496**, 14–19.
17 J. Waluk, in *Handbook of Porphyrin Science*, ed. K. Smith, K. Kadish and R. Guilard, World Scientific, Singapore, 2010, vol. 7, pp. 359–436.
18 Ł. Walewski, J. Waluk and B. Lesyng, *J. Phys. Chem. A*, 2010, **114**, 2313–2318.
19 M. Gil, J. Dobkowski, G. Wiosna-Sałyga, N. Urbańska, P. Fita, C. Radzewicz, M. Pietraszkiewicz, P. Borowicz, D. Marks, M. Glasbeek and J. Waluk, *J. Am. Chem. Soc.*, 2010, **132**, 13472–13485.
20 A. Vdovin, J. Waluk, B. Dick and A. Slenczka, *ChemPhysChem*, 2009, **10**, 761–765.
21 J. Lopez del Amo, U. Langer, V. Torres, M. Pietrzak, G. Buntkowsky, H. M. Vieth, M. F. Shibl, O. Kühn, M. Bröring and H. H. Limbach, *J. Phys. Chem. A*, 2009, **113**, 2193–2206.
22 P. Fita, N. Urbańska, C. Radzewicz and J. Waluk, *Chem.–Eur. J.*, 2009, **15**, 4851–4856.
23 J. Waluk, *Pol. J. Chem.*, 2008, **82**, 947–962.
24 Z. Smedarchina, W. Siebrand, A. Fernandez-Ramos and R. Meana-Paneda, *Z. Phys. Chem. (Muenchen, Ger.)*, 2008, **222**, 1291–1309.
25 P. Fita, N. Urbańska, C. Radzewicz and J. Waluk, *Z. Phys. Chem.*, 2008, **222**, 1165–1173.
26 J. Waluk, in *Hydrogen-Transfer Reactions*, ed. J. T. Hynes, J. P. Klinman, H. H. Limbach and R. L. Schowen, Wiley-VCH, Weinheim, 2007, vol. 1, pp. 245–271.
27 Z. Smedarchina, M. F. Shibl, O. Kühn and A. Fernández-Ramoz, *Chem. Phys. Lett.*, 2007, **426**, 314–321.
28 M. Pietrzak, M. F. Shibl, M. Bröring, O. Kühn and H. H. Limbach, *J. Am. Chem. Soc.*, 2007, **129**, 296–304.
29 M. Gil and J. Waluk, *J. Am. Chem. Soc.*, 2007, **129**, 1335–1341.
30 J. Waluk, *Acc. Chem. Res.*, 2006, **39**, 945–952.
31 A. Vdovin, J. Sepioł, N. Urbańska, M. Pietraszkiewicz, A. Mordziński and J. Waluk, *J. Am. Chem. Soc.*, 2006, **128**, 2577–2586.
32 P. Fita, P. Garbacz, M. Nejbauer, C. Radzewicz and J. Waluk, *Chem.–Eur. J.*, 2011, **17**, 3672–3678.
33 H. Piwoński, A. Hartschuh, N. Urbańska, M. Pietraszkiewicz, J. Sepioł, A. Meixner and J. Waluk, *J. Phys. Chem. C*, 2009, **113**, 11514–11519.
34 M. K. Abdel-Latif and O. Kühn, *Theor. Chem. Acc.*, 2011, **128**, 307–316.
35 M. F. Shibl, M. Pietrzak, H. H. Limbach and O. Kühn, *ChemPhysChem*, 2007, **8**, 315–321.
36 M. F. Shibl, M. Tachikawa and O. Kühn, *Phys. Chem. Chem. Phys.*, 2005, **7**, 1368–1373.
37 R. M. Gulam, T. Matsushita, S. Neya, N. Funasaki and J. Teraoka, *Chem. Phys. Lett.*, 2002, **357**, 126–130.
38 R. M. Gulam, T. Matsushita and J. Teraoka, *J. Phys. Chem. A*, 2003, **107**, 2172–2178.
39 R. M. Gulam, S. Neya and J. Teraoka, *J. Porphyrins Phthalocyanines*, 2006, **10**, 1271–1284.
40 M. G. Rabbani and J. Teraoka, *Spectrochim. Acta, Part A*, 2010, **76**, 207–212.
41 N. Urbańska, M. Pietraszkiewicz and J. Waluk, *J. Porphyrins Phthalocyanines*, 2007, **11**, 596–600.
42 E. Vogel, M. Köcher, H. Schmickler and J. Lex, *Angew. Chem., Int. Ed. Engl.*, 1986, **25**, 257–259.
43 J. P. Toennies and A. F. Vilesov, *Annu. Rev. Phys. Chem.*, 1998, **49**, 1–41.

44 J. P. Toennies and A. F. Vilesov, *Angew. Chem., Int. Ed.*, 2004, **43**, 2622–2648.
45 M. Leverenz, B. Schilling and J. P. Toennies, *Chem. Phys. Lett.*, 1993, **206**, 381–387.
46 NIST Atomic Spectra Database (version 3.1.5), http://physics.nist.gov/asd3. National Institute of Standards and Technology, Gaithersburg, MD, USA.
47 http://www.ill.eu/instruments-support/instruments-groups/instruments/in4/.
48 http://www.ill.eu/instruments-support/instruments-groups/instruments/in1/.
49 http://www.ill.eu/instruments-support/computing-for-science/cs-software/all-software/lamp/the-lamp-book/.
50 CPMD version 3.13.2, http://www.cpmd.org/, Copyright IBM Corp. 1990–2008, Copyright MPI für Festkörperforschung Stuttgart 1997–2001.
51 A. D. Becke, *Phys. Rev. A*, 1998, **38**, 3098–3100.
52 C. L. Lee, W. Yang and R. G. Parr, *Phys. Rev. B: Condens. Matter*, 1988, **37**, 785–789.
53 N. Troullier and J. L. Martins, *Phys. Rev. B: Condens. Matter*, 1991, **43**, 1993–2006.
54 R. W. Hockney, *Methods Comput. Phys.*, 1970, **9**, 135–211.
55 G. J. Martyna, M. L. Klein and M. Tuckerman, *J. Chem. Phys.*, 1992, **97**, 2635–2643.
56 R. Ramirez, T. Lopez-Ciudad, P. Kumar and D. Marx, *J. Chem. Phys.*, 2004, **121**, 3973–3983.
57 P. M. Kozlowski, A. A. Jarzcki and P. Pulay, *J. Phys. Chem.*, 1996, **100**, 7007–7010.
58 P. M. Kozlowski, A. A. Jarzcki, P. Pulay, X.-Y. Li and M. Z. Zgierski, *J. Phys. Chem.*, 1996, **100**, 13985–13992.
59 N. Verdal, P. M. Kozlowski and B. S. Hudson, *J. Phys. Chem. A*, 2005, **109**, 5724–5733.
60 D. C. Bieńko, D. Michalska, S. Roszak, W. Wojciechowski, M. J. Nowak and L. Lapinski, *J. Phys. Chem. A*, 1997, **101**, 7834–7841.
61 L. Lapinski, M. J. Nowak, D. C. Bieńko and D. Michalska, *Phys. Chem. Chem. Phys.*, 2002, **4**, 1123–1128.
62 T. Stepanenko, L. Lapinski, M. J. Nowak, J. S. Kwiatkowski and J. Leszczynski, *Spectrochim. Acta, Part A*, 2001, **57**, 375–383.
63 S. Gawinkowski, J. Eilmes and J. Waluk, *J. Mol. Struct.*, 2010, **976**, 215–225.
64 J. Radziszewski, M. Nepraš, V. Balaji, J. Waluk, E. Vogel and J. Michl, *J. Phys. Chem.*, 1995, **99**, 14254–14260.
65 J. G. Radziszewski, J. Waluk and J. Michl, *Chem. Phys.*, 1989, **136**, 165–180.
66 S. F. Mason, *J. Chem. Soc.*, 1958, 976–982.
67 M. D. Halls, J. Velkovski and H. B. Schlegel, *Theor. Chem. Acc.*, 2001, **105**, 413–421.
68 A. Starukhin, E. Vogel and J. Waluk, *J. Phys. Chem. A*, 1998, **102**, 9999–10006.
69 G. J. Martyna and M. E. Tuckerman, *J. Chem. Phys.*, 1999, **110**, 2810–2821.